Calculating the electrostatic properties of RNA provides new insights into molecular interactions and function

Kevin Chin[1], Kim A. Sharp[2], Barry Honig[1] and Anna Marie Pyle[1,3]

Solutions to the nonlinear Poisson-Boltzmann equation were used to obtain the electrostatic potentials of RNA molecules that have known three-dimensional structures. The results are described in terms of isopotential contours and surface electrostatic potential maps. Both representations have unexpected features: 'cavities' within isopotential contours and areas of enhanced negative potential on molecular surfaces. Intriguingly, the sites of unusual electrostatic features correspond to functionally important regions, suggesting that electrostatic properties play a key role in RNA recognition and stabilization. These calculations reveal that the electrostatic potentials generated by RNA molecules have a variety of functionally important characteristics that cannot be discerned by simple visual inspection of the molecular structure.

Results and discussion

The role of electrostatics in molecular interactions of proteins has been well established in a number of studies[1]. These have revealed that the surfaces of proteins are covered with distinct patches of electrostatic potential which play important roles in molecular recognition[2]. Unlike proteins, nucleic acids contain only negatively charged residues and these are uniformly distributed throughout the polymer. It is therefore difficult to envision how distinct regions of electrostatic potential are generated and how these might contribute to stabilizing interactions between nucleic acid molecules.

Now that a variety of new RNA structures are available[3], it is possible to examine more generally the links between RNA structural form and electrostatic function. In this study, electrostatics calculations are used to accomplish two fundamental objectives. First, the electrostatic potential contours surrounding RNA structures are visualized and described in an effort to understand the electrostatic basis for association between two RNA molecules or domains of RNA tertiary structure. Second, surface potentials are calculated in an attempt to identify heterogeneities, or patches of positive and negative potential along the RNA surface. It is of particular interest to determine whether there are unique patterns of electrostatic potential that lead to strong sites of metal ion association (or other types of molecular recognition) and whether these can be predicted computationally.

The calculations described here are based on numerical solutions to the nonlinear Poisson-Boltzmann equation (NLPB). Due to the high charge density of nucleic acids, the complete NLPB is required for calculating electrostatics rather than the linearized equation (LPB) that has generally been adequate for most proteins[4]. With the exception of a single study on $tRNA^{phe}$ (ref. 5), the NLPB has not been applied previously for calculating the electrostatic properties of RNA

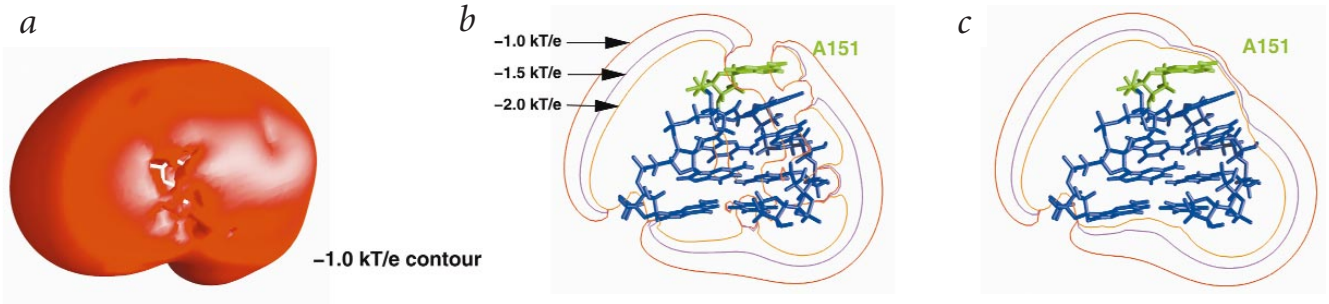

Fig. 1 Isopotential contours of a GNRA tetraloop and its receptor. ***a***, Overhead view of a three-dimensional isopotential contour of the GNRA tetraloop from P456 (ref. 13) at -1.0 kT/e. There is a hole over the second base of the tetraloop (A151, represented as the white base). ***b***, Side view of two-dimensional isopotential contours of the GNRA tetraloop, using charges on all atoms. Contours are at levels of -1.0 kT/e (red), -1.5 kT/e (purple), and -2.0 kT/e (orange). The hole over A151 (green base) is clearly visible. Note that the contours near the isopotential hole are collapsing, indicating an increase in the local field. ***c***, Two-dimensional isopotential contours of the GNRA tetraloop, using charges only on the phosphates. The overall shape of the isopotential contours is relatively unchanged. The potential hole has disappeared but the contours are still collapsed near A151. This indicates that charges on the phosphates are the major contributor to contour shape, but bases are responsible for creating or exacerbating holes.

[1]Department of Biochemistry and Molecular Biophysics, Columbia University, 630 West 168th Street, Box 36, New York, New York 10032, USA. [2]Department of Biochemistry and Biophysics, University of Pennsylvania, Room 417 Anatomy Chemistry Building, Philadelphia, Pennsylvania 19104, USA. [3]Howard Hughes Medical Institute, Columbia University, New York, New York, USA.

Correspondence should be addressed to A.M.P. *email: amp11@columbia.edu* or B.H. *email: bh6@columbia.edu*

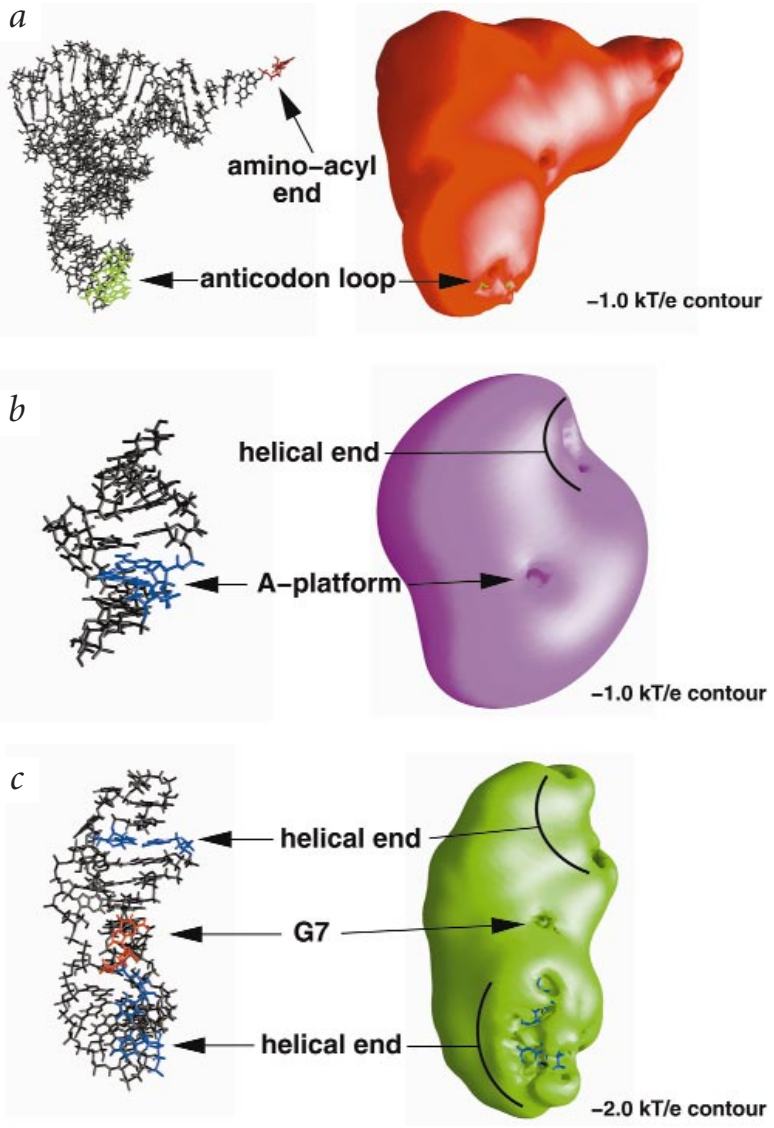

Fig. 2 Three-dimensional isopotential contours of various RNA structures. ***a***, Three-dimensional isopotential contour of yeast $tRNA^{phe}$ at -1.0 kT/e. As previously observed[5] there is a potential hole over the anticodon loop (green bases) and the acylation end (red base) of the tRNA. ***b***, Three-dimensional isopotential contour of the GNRA tetraloop receptor from P456 at -1.0 kT/e. A hole is visible at the sugar of the 3' adenosine of the A-platform motif (represented as blue bases on the left). This hole corresponds to a site above A151, though it is not exactly aligned with the hole seen in the tetraloop. The positioning of the two holes may indicate that the structures have adopted shapes that will minimize repulsive forces when they interact. The top right of the contour also shows a hole that corresponds to the end of the double helix (helical end). All helical ends display such large potential holes. ***c***, Three-dimensional isopotential contours of a pseudoknot that promotes efficient ribosomal frameshifting of MMTV at -2.0 kT/e. This pseudoknot[18] has a potential hole over G7 (represented as a red base on the left) of its sequence. This residue is found in the two nucleotide loop 1, which generates a bend in the pseudoknot. As seen in (*b*), the helical ends (blue bases on the left) have potential holes over them.

molecules. NLPB calculations have been shown to provide accurate descriptions of electrostatic effects in other nucleic acid systems[2,6]. Calculated effects are consistent with potential measurements from EPR techniques[7], observed salt dependencies for the binding of ligands and proteins to DNA[8,9] and measured pK_a shifts induced by binding to DNA[10]. Thus, the results presented herein are likely to provide a realistic description of the electrostatic potentials surrounding RNA molecules.

Testing the parameters used in electrostatics calculations

In order to relate the current study to earlier work, electrostatic potentials around $tRNA^{phe}$ (PDB: 1tra)[11] were computed and compared with previous calculations on the same system[5]. In both sets of calculations, clear potential holes over the anticodon region and the 3' acylation end were observed. Like the anticodon of $tRNA^{phe}$, GNRA tetraloops adopt a U-turn structure[12]. To determine if the electrostatic properties of U-turns are general, isopotential contours were calculated from a typical structure of a GAAA tetraloop motif (PDB: 1gid)[13]. Analysis of the results reveals a large potential hole over the second base of the loop, similar to the one seen at the anticodon loop of tRNA (compare Fig. 1*a,b* with Fig. 2*a*).

Since the partial charges assigned to atoms in RNA will have an effect on electrostatics, two different sets of charges, from the force fields Cornell'95 (AMBER)[14] and cvff91 (Biosym/MSI), were applied in calculations on the GAAA tetraloop structure. A comparison of the isopotential contours generated using each force field revealed that there are only minor differences in the calculated results (data not shown). In order to test the sensitivity of the results to details of the charge distribution, a series of calculations were performed in which charges were placed only on the phosphates of the tetraloop. This results in disappearance of the potential hole at -1.0 to -2.0 kT/e contour levels (Fig. 1*c*). The cavity can still be seen at more negative isopotential contour levels, which is consistent with previous results on yeast $tRNA^{phe}$ (ref. 5). These results indicate that the charge distribution on the bases is partially responsible for cavities in the isopotential contours.

It is well established that the shape of the interface between a low dielectric macromolecule and a high dielectric solvent is essential for determining the shape of an electrostatic potential contour[2,15]. In order to observe this effect in the context of the present work, a calculation was carried out in which the molecular dielectric constant was set at 80, thus removing the discontinuity in the dielectric constant. This results in isopotential contours that roughly follow the van der Waals surface of the macromolecule and cavities are not observed (data not shown).

A structure can relax during the course of binding or conformational changes, resulting in a higher interior dielectric constant[16,17]. We have therefore studied whether large variations in the interior dielectric constant have significant effects on the overall results of electrostatics calculations. As the interior dielectric constant was increased, the size of the potential holes decreased but they were still apparent at dielectric values as high as 20 (data not shown). Thus, the results presented herein are basically independent of the exact value assigned to the interior dielectric constant.

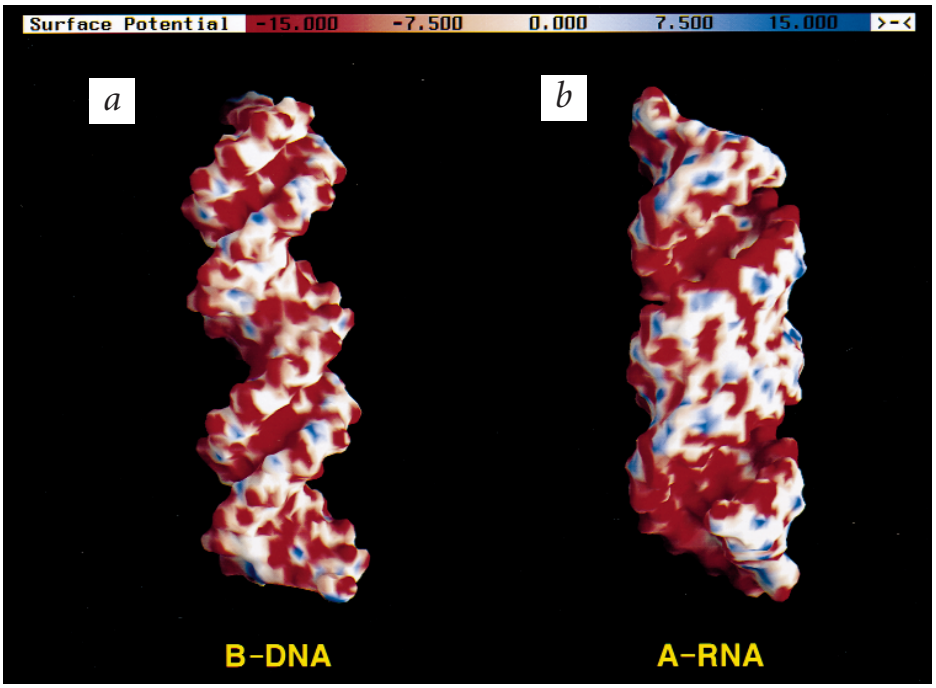

Fig. 3 Surface potentials of standard forms of nucleic acids with identical sequences. ***a***, B-DNA helix. The minor groove has significantly more negative potential (-15 to -25 kT/e) than does the major groove (-5 to -10 kT/e), in agreement with previous observations[29]. ***b***, A-RNA helix. The major groove has more negative potential (-15 to -20 kT/e) than the minor groove (-5 to -10 kT/e)[44]. The scale at the top of the figure is in units of kT/e.

Isopotential contours of common, functionally important RNA motifs

Given that there are interesting features in the isopotential contours of the GAAA tetraloop, it was important to examine the electrostatic properties of other common RNA structural motifs. NLPB calculations were performed on several RNA crystal structures, including a simple duplex RNA, the GAAA tetraloop receptor (PDB: 1gid)[13], the MMTV pseudoknots (PDB: 1rnk, 1kpd)[18,19], and the sarcin–ricin loop (PDB: 1scl)[20]. Pronounced cavities were observed at specific positions in the isopotential contours of each molecule: potential holes were consistently observed over the bases at helical termini (Fig. 2*b*,*c*); over the A-A platform of the tetraloop receptor (Fig. 2*b*); over G7 of the MMTV pseudoknots (Fig. 2*c*) and over G10 of the sarcin–loop (data not shown).

In each case, cavities in the isopotential contours occurred at positions where the RNA interacts with another RNA molecule (as in helical termini, the anticodon loop of $tRNA^{phe}$; the N position of the GNRA tetraloop motif[13]; and the A-platform of the GAAA tetraloop receptor[21]) or with certain types of protein domains (the GNRA tetraloop[22,23], and G10 of the sarcin–ricin loop[20]). It has been suggested that coaxial stacking of separate helices is one of the most important early events in RNA tertiary folding[24], an hypothesis that is supported by the pronounced cavity in the isopotential contour centered over helical termini. Similarly, GNRA tetraloops interact with A-platforms and with aromatic side chains of proteins at the N-position[13,22,23], directly beneath a cavity in the isopotential contour. Cavities observed at G7 of the MMTV pseudoknots occur at the position where pseudoknots bend, at a site involved in ribosome recognition[25]. This correlation between sites of cavities and sites of intermolecular interaction suggests that the potential holes help to minimize electrostatic repulsion between macromolecules, thus facilitating or stabilizing interactions. The existence of these cavities and their dependence on molecular shape suggests that the structure of an RNA may have evolved, in part, to modulate the electrostatic properties of the molecule.

The significance of cavities in RNA isopotential contours

For the cavities to promote intermolecular interactions of RNA, the extent to which they minimize repulsion must be energetically significant. The repulsive free energy from charge–charge interactions associated with bringing a single negative charge from infinity to the -1 kT/e contour is +1 kT. The isopotential hole over the GAAA loop indicates that the electrostatic resistance to the approach of another RNA coming from directly above is reduced, even at the interaction distance of 3–4 Å (data not shown). In contrast, there is significant repulsion if the RNA approaches from a different orientation (Fig. 1*b*). In addition to these charge–charge effects, there will be an electrostatic repulsion arising from displacement of the high dielectric solvent by the other low dielectric RNA molecule (the image charge effect)[26].

Potential holes often occur at positions of extrahelical bases, which tend to be further away from the sugar–phosphate backbone than other positions within a nucleic acid structure. However, it should be noted that not all flipped out bases or helical ends are sites of potential holes. For example, UNCG tetraloops generally have the second and third base flipped out from the backbone (PDB: 1ebq)[27]. However, in contrast to GNRA loops, these bases generally flip back toward the interior of the molecule, and no potential hole is formed. Interestingly, GNRA loops participate in tertiary interactions with other molecules while UNCG loops do not.

Surface potentials of RNA molecules

In addition to isopotential contours, which describe the potential some distance from the molecule, it has also proven useful to represent regions of enhanced electrostatic potential on the molecular surface. This second representation makes it possible to correlate certain regions of the surface with specific electrostatic characteristics. Using GRASP[28], regions of positive surface charge are represented in blue and regions of negative charge are represented in red (neutral is white).

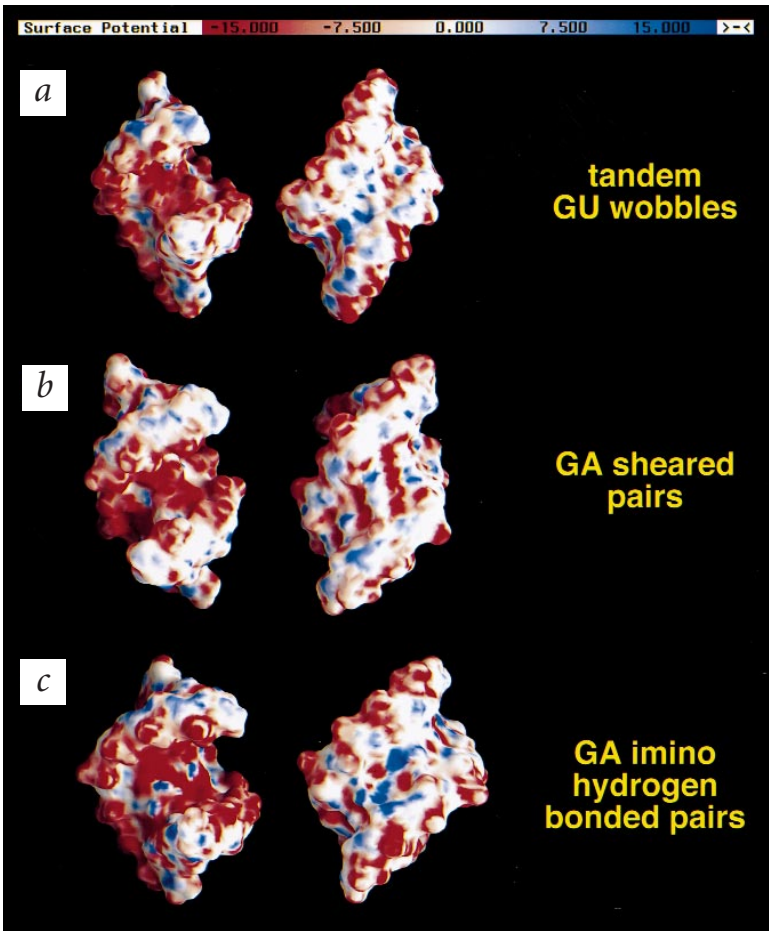

Fig. 4 Surface potentials of helices containing internal base pair mismatches. ***a***, Surface potentials of a helix containing tandem G-U wobble base pairs. The major groove is slightly negative (left, from -10 to -20 kT/e) and the minor groove is slightly positive (right, from +10 to +15 kT/e). Although the major groove potential is similar to that of standard A-form, its uniformity and the lack of any strong positive charges in the major groove may make the tandem G-U wobble an effective metal binding site. ***b***, Surface potentials of a helix containing tandem sheared G-A base pairs. The major groove is very negative (left, from -20 to -30 kT/e) and the minor groove is slightly negative (right, from -15 to -20 kT/e). The sheared G-A motif is a known metal binding motif found in many RNA structures[13,34,45]. The sheared motif also provides several possible contacts with base atoms not involved in pairing. ***c***, Surface potentials of a helix containing tandem imino hydrogen bonded G-A base pairs. The major groove is very negative (left, from -15 to -25 kT/e) but also contains areas of strong positive potential (left, from +15 to +20 kT/e). The same is true of the minor groove (right, as negative as -20 kT/e and as positive as +20 kT/e). The mixture of potentials at close range would make it difficult for a simple electrostatic interaction to prevail at this motif.

Major electrostatic features of A- and B-form helices

Electrostatic features in the major and minor grooves of nucleic acid helices have long been the subject of investigation since they have important ramifications for drug and counterion binding. NLPB calculations reveal that the minor groove of a regular B-form DNA helix is significantly more negative (normally ranging from -15 to -25 kT/e) than the major groove (-5 to -10 kT/e) (Fig. 3*a*), particularly at A-T rich sequences. This is consistent with previous calculations[29] and the finding that cationic DNA binding drugs prefer to interact with the minor groove of B-DNA due to its greater negative electrostatic potential[30,31].

By comparison, it was of interest to examine the electrostatic properties of A-form nucleic acids, and to compare properties of both A-form RNA and DNA helices. An analysis of the surface potentials on both A-form helices, in contrast to B-DNA, show that the major groove is much more negative (-15 to -20 kT/e) than the minor groove (-5 to -10 kT/e), although both grooves display patches of both positive and negative potential (Fig. 3*b*). This is consistent with the observation that divalent metal ions tend to bind in the major groove of RNA[32–36]. Only minor differences were observed between the electrostatic features of A-form RNA and DNA of the same sequence (data not shown). When full negative charges are placed only on the phosphates of an A-form helix, the major groove has a uniformly greater negative potential than the minor groove. However, when charges on each atom are included, there is some sequence-dependent variability in this pattern (data not shown). This heterogeneity is likely to be significant, and could play an important role in molecular recognition.

Surface potentials of common non-Watson-Crick base pairs

It is becoming increasingly evident that non-Watson Crick base pairs play an important role in the function of nucleic acids and of RNA in particular. The most common non-Watson-Crick RNA interaction is the G-U base pair. Surface potential analysis of an RNA containing tandem G-U wobble base pairs (PDB: 1qes)[37] reveals that the major groove of the helix is more uniformly negative and the minor groove is actually positive at the tandem pair (Fig. 4*a*). Thus, tandem G-U wobble base pairs are a likely target for metal binding, as previously reported[13].

The G-A mismatch exists in two different conformations, sheared (PDB: 1yfv)[38] and imino hydrogen bonded (PDB: 1mis)[39]. Surface potential analysis of the sheared conformation reveals an increase in the negative electrostatic potential in both the major and minor grooves (Fig. 4*b*). The widened minor groove also displays a more negative character (-25 to -30 kT/e) when compared to a normal helix. Although there are some electrostatic similarities to the sheared conformation, in the imino hydrogen bonded form both the major and minor grooves have areas of positive and negative potential, making electrostatic features more complex (Fig. 4*c*).

Surface potentials of RNA tertiary structures

The NLPB was used to calculate the electrostatic surface potentials of RNA molecules that have unique structural features or a complex tertiary architecture. In particular, it was of interest to determine if localized regions of negative electrostatic potential correspond to metal ion binding sites. Note that water molecules and metal ions were explicitly not included in the calculations. Analysis of the $tRNA^{phe}$ molecule (PDB: 1tra)[11] revealed a structure with electrostatic properties that are typical of RNA helices, although there are distinct pockets in the molecule that are characterized by exceptionally negative electrostatic potential which correspond to three of the strong metal binding sites in tRNA[11,40] (data not shown). Analysis of the P456 domain from the *Tetrahymena* group I intron (PDB: 1gid)[13] revealed an abundance of interesting

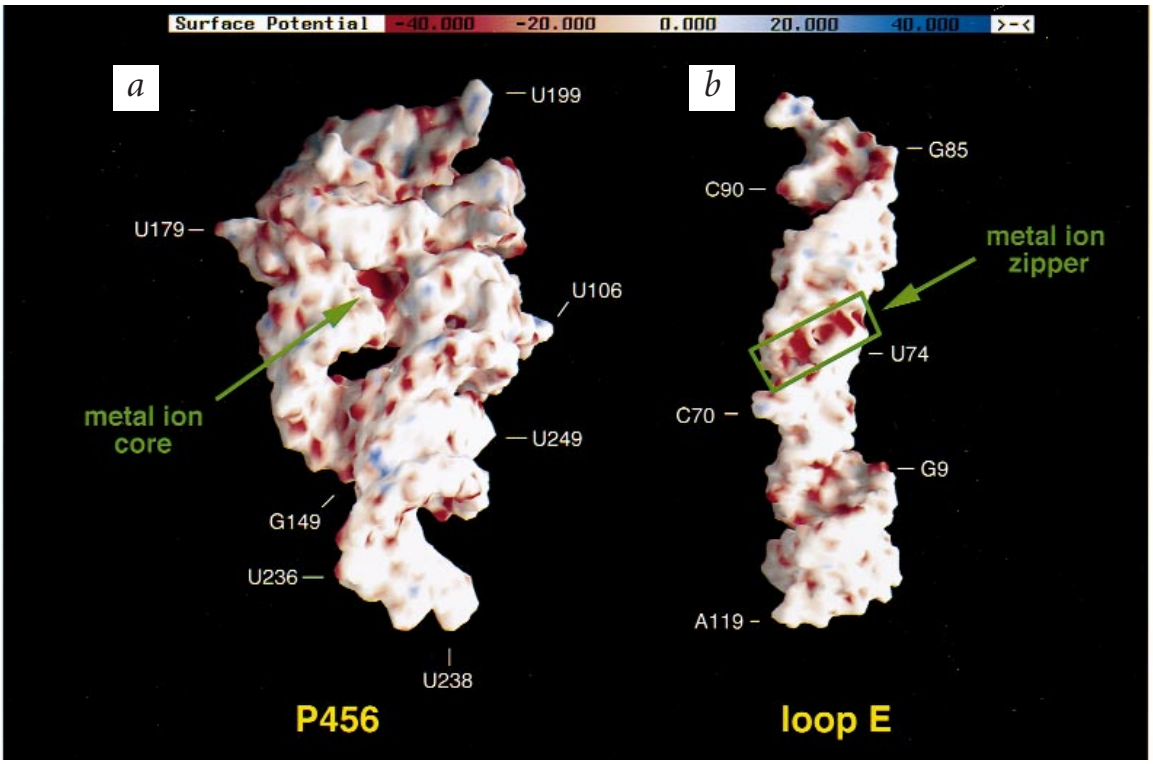

F ig. 5 Surface potentials of large RNAs with known metal binding sites. ***a***, Surface potentials of P456 of the *Tetrahymena* group I intron. The ionic strength used in solving the NLPB for this molecule was 0.25 M, because at 0.145 M the solver was unable to converge. The metal ion core of P456 is clearly visible as the red patch (potentials ranging from -80 to -100 kT/e) at the center. It is significantly more negative than the rest of the molecule (potentials ranging from -5 to -30 kT/e). ***b***, Surface potentials of loop E of 5S rRNA. The metal zipper of 5S rRNA is clearly visible (green box) as a series of red patches (potentials of -50 to -80 kT/e) as compared with the rest of the molecule (potentials ranging from -5 to -20 kT/e). This motif, consisting of purine-purine and G-U base pairs, is accompanied by a narrowing of the major groove of the helix.

electrostatic features. Like tRNA, most of the molecule has electrostatic character similar to that of simple helices. However in the center of the molecule there is a region with extremely negative electrostatic potential (-80 to -100 kT/e) that corresponds precisely to the position of the 'metal ion core' in P456 (Fig. 5). Finally, NLPB calculations on the loop E structure from *E. coli* 5S rRNA (PDB: 364d)[34] reveal a major groove section of unusually negative electrostatic potential corresponding to the site of the 'metal ion zipper' previously reported from crystallographic studies (Fig. 5). Therefore, in each case, surface potential analysis was able to predict the position of metal ion binding sites that had been identified crystallographically.

Predicting metal ion binding sites in RNA

Given that surface potential calculations were capable of predicting known metal-binding sites, it was of interest to determine if the calculations might reveal unreported metal ion binding sites. To this end, the GAAA tetraloop–receptor region of the P456 crystal structure was examined in isolation for regions of unusually negative electrostatic potential. The individual tetraloop and receptor regions do not show pockets of negative potential. However, when they are bound together in the tetraloop–receptor motif, a small region of densely negative potential (-30 to -60 kT/e) becomes apparent (Fig. 6). The site is large enough to accommodate a Mg^{2+} coordinated through inner-sphere contacts. The residues surrounding this small hole in the structure include A153 and C154 of the tetraloop plus C223 and G251 of the receptor. Another small pocket of highly negative potential (-30 to -40 kT/e), involves tetraloop residues A151 and A152 and the A225 phosphate of the receptor (data not shown).

Although metal ions have been studied extensively with respect to their roles in RNA catalysis and folding[24,41] it has been difficult to define the exact locations of Mg^{2+} or monovalent ions within RNA structures[3]. A study of RNA surface potentials can therefore provide a useful method for identifying likely sites of metal ion binding in a known structure. The identification of ion binding sites in yeast $tRNA^{phe}$ (ref. 11), P456 of the group I intron[13], and *E. coli* 5S rRNA[34] indicates that calculation of surface potential is a viable method for metal ion site prediction and for analysis of those sites. The NLPB method described herein is complementary to the more computationally intensive prediction of metal ion binding sites using Brownian dynamics simulations[42], in which metals sample different regions of the RNA molecular surface before settling down into a putative metal binding site.

A new way of visualizing RNA

The biological function of a macromolecule is profoundly influenced by the electrostatic field projecting into the solution and the electrostatic features on the molecular surface. These features cannot be inferred by simply looking at the molecular structure of an RNA. NLPB calculations on crystal structures and models of RNA structure combine information about molecular shape and individual atomic charges to provide a new way of 'seeing' RNA. They show that RNA molecules are surrounded by electrostatic potential contours

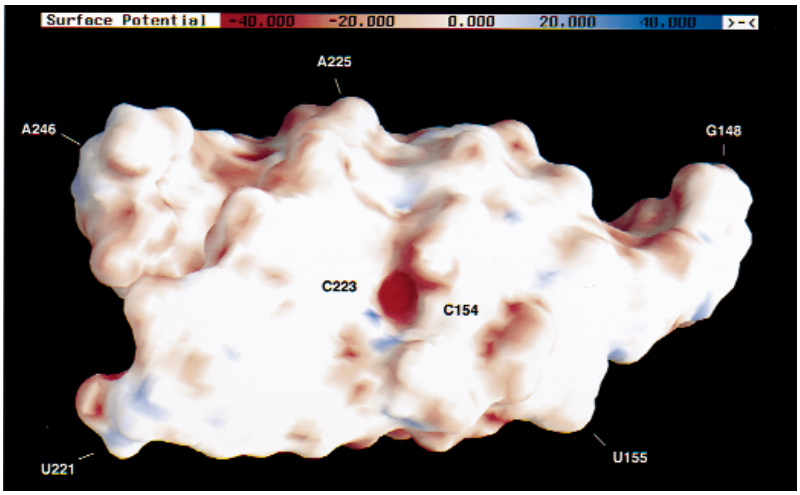

Fig. 6 Surface potentials of the tetraloop–receptor interaction. A negative pocket, ranging from -30 to -60 kT/e, that is more negative than its surrounding region (potentials from -5 to -10 kT/e) is formed between the two interacting molecules. The residues involved are A153 and C154 of the tetraloop plus C223 and G251 of the receptor.

having unique shapes that do not necessarily follow contours of the molecular surface. The topologies of these contours help to explain, in every instance examined, the biological function of individual RNA molecules. Electrostatics calculations also provide a means for determining the magnitude of potential at specific regions on the molecular surface. As shown in this paper, one can now visualize regions of unusually positive or negative potential on RNA molecules in the manner that has now become commonplace for the analysis of protein structures.

Methods

Structures and programs. Coordinates of RNA structures were obtained from the Protein Data Bank (PDB; http://www.rcsb.org/pdb) or from the Nucleic Acid Database (NDB; http://ndb.rutgers.edu). Structures are identified by their PDB codes. Three-dimensional structures were displayed using GRASP[28] or Insight II (Biosym/MSI). Hydrogen atoms were added to the X-ray structures via the Biopolymer module of Insight II. Bound water molecules and metal ions were not included in the calculations.

Solutions to the NLPB. Numerical solutions to the NLPB were obtained from a finite difference multigridding algorithm that has now been incorporated into the DelPhi program. The NLPB is given by:

$$\nabla\cdot[\varepsilon(\mathbf{r})\nabla\cdot\phi(\mathbf{r})] - (8\pi e^2 I / kT)\sinh[\phi(\mathbf{r})] + 4\pi e\rho^f(\mathbf{r}) / kT = 0 \qquad (1)$$

where ϕ is the dimensionless electrostatic potential in units of kT/e, k is Boltzmann's constant, T is the absolute temperature, e is the proton charge, ε is the dielectric constant, ρ^f is the fixed charge density, and I is the ionic strength of the bulk solution. The quantities ϕ, ε, and ρ are all functions of the position vector $\mathbf{r}$ in the reference frame centered on a fixed macromolecule.

Variable parameters. The AMBER (Oxford Molecular) and DISCOVER (Biosym/MSI) molecular simulation programs use parameter sets (force fields) that describe atomic size and partial charges of the atoms in RNA molecules. Except for tRNA, the more recent force field found in AMBER, Cornell'95 (ref. 14), is used throughout this paper. The DISCOVER force field, cvff91 (Biosym/MSI), is used as a control parameter set and for calculations on tRNA, which contains modified nucleotides that are not accounted for in the AMBER charge set. The RNA molecule is treated as a low dielectric medium (ε_m) within the volume enclosed by the molecular surface of the macromolecule (probe radius = 1.4 Å). As has been discussed extensively with regard to proteins[26], a dielectric constant of 2 accounts well for the effect of electronic polarizability. The dielectric constant of nucleic acids is also expected to be small since base pairing, base stacking, and steric interactions will restrict dipolar fluctuations within the double helix[10]. Unless otherwise stated, an interior dielectric constant of 2 was used in the calculations. The surrounding solvent was treated as a continuum of dielectric constant (ε_s) 80 with a 1:1 electrolyte distributed according to a Boltzmann weighted average of the mean electrostatic potential. A 2.0 Å ion exclusion radius (corresponding roughly to the hydrated radius of a sodium ion) was added to the surface of the macromolecules to account for ion size. For the calculations presented here, a univalent salt concentration of 0.145 M (physiological ionic strength) was used. The exception is for the P456 group I intron domain[13], for which the program was able to converge the NLPB only at 0.25 M salt concentrations or higher.

In order to obtain numerical solutions to equation 1 it is first necessary to map the molecular system onto a three-dimensional lattice. Since the lattice is necessarily finite, potentials at the boundaries of the lattice are not trivially defined. Initial calculations were done to approximate the potentials at the lattice points on the boundary of the grid using the Debye-Hückel equation[15]. To further improve the accuracy of potentials, a simple focusing procedure was used[43].

Visualization of potentials. The calculated electrostatic potentials are displayed using the GRASP program[28]. Isopotential contours at a level of -1 kT/e are displayed in most of the figures although in some cases more negative contours are displayed. Since RNA molecules bear a large negative charge most of the molecular surface has a negative electrostatic potential. Using the standard GRASP color code, this would result in almost the entire surface being displayed in a red color. In order to avoid this, the color mapping of the potential was scaled as indicated so that only the most negative areas are displayed as red.

Available programs. The NLPB solver program, sample parameter files, and a short tutorial on using the program are available at: http://cpmcnet.columbia.edu/dept/gsas/biochem/labs/pyle/electrostatics.html.

Acknowledgments

We are grateful to C. Duarte and B. Hitz for helpful discussions and to E. Jankowsky for critical review of the manuscript. We thank S. Sridharan for assistance in modifying the NLPB solver program. This work was supported by a NYI award to A.M.P. from the NSF and an NIH grant to B.H. A.M.P. is an assistant investigator of the Howard Hughes Medical Institute.

Received 16, June, 1999; accepted 31, August, 1999.

1 Sharp, K.A. & Honig, B. Electrostatic interactions in macromolecules: theory and applications. *Annu. Rev. Biophys. Biophys. Chem.* **19**, 301–332 (1990).
2. Honig, B. & Nicholls, A. Classical electrostatics in biology and chemistry. *Science* **268**, 1144–1149 (1995).
3. Uhlenbeck, O.C., Pardi, A. & Feigon, J. RNA structure comes of age. *Cell* **90**, 833–840 (1997).
4. Madura, J.D. *et al.* Biological applications of electrostatic calculations and Brownian dynamics simulations. *Rev. Comput. Chem.* **5**, 229–267 (1994).
5. Sharp, K.A., Honig, B. & Harvey, S.C. Electrical potential of transfer RNAs: codon-anticodon recognition. *Biochemistry* **29**, 340–346 (1990).
6. Sharp, K.A. & Honig, B. Salt effects on nucleic acids. *Curr. Opin. Struct. Biol.* **5**, 323–328 (1995).
7. Sharp, K.A., Friedman, R.A., Misra, V., Hecht, J. & Honig, B. Salt effects on polyelectrolyte-ligand binding: comparison of Poisson-Boltzmann, and limiting law/counterion binding models. *Biopolymers* **36**, 245–262 (1995).
8. Misra, V.K., Sharp, K.A., Friedman, R.A. & Honig, B. Salt effects on ligand-DNA binding. Minor groove binding antibiotics. *J. Mol. Biol.* **238**, 245–263 (1994).
9. Misra, V.K., Hecht, J.L., Sharp, K.A., Friedman, R.A. & Honig, B. Salt effects on protein–DNA interactions. The λcI repressor and EcoRI endonuclease. *J. Mol. Biol.* **238**, 264–280 (1994).
10. Misra, V.K., Hecht, J.L., Yang, A. & Honig, B. Electrostatic contributions to the binding free energy of the λcI repressor to DNA. *Biophys. J.* **75**, 2262–2273 (1998).
11. Westhof, E. & Sundaralingam, M. Restrained refinement of the monoclinic form of yeast phenylalanine transfer RNA. Temperature factors and dynamics, coordinated waters, and base-pair propeller twist angles. *Biochemistry* **25**, 4868–4878 (1986).
12. Jucker, F.M. & Pardi, A. GNRA tetraloops make a U-turn. *RNA* **1**, 219–222 (1995).
13. Cate, J.H. *et al.* Crystal structure of a Group I ribozyme domain: Principles of RNA packing. *Science* **273**, 1678–1685 (1996).
14. Cornell, W.D. *et al.* A second generation force field for the simulation of proteins, nucleic acids, and organic molecules. *J. Am. Chem. Soc.* **117**, 5179–5197 (1995).
15. Klapper, I., Hagstrom, R., Fine, R., Sharp, K. & Honig, B. Focusing of electric fields in the active site of Cu-Zn superoxide dismutase: effects of ionic strength and amino-acid modification. *Proteins* **1**, 47–59 (1986).
16. Gilson, M. & Honig, B. The dielectric constant of a folded protein. *Biopolymers* **25**, 2097–2119 (1986).
17. Yang, L., Weerasinghe, S., Smith, P.E. & Pettitt, B.M. Dielectric response of triplex DNA in ionic solution from simulations. *Biophys. J.* **69**, 1519–1527 (1995).
18. Shen, L.X. & Tinoco, I. The structure of an RNA pseudoknot that causes efficient frameshifting in mouse mammary-tumor virus. *J. Mol. Biol.* **247**, 963–978 (1995).
19. Kang, H. & Tinoco, I. A mutant RNA pseudoknot that promotes ribosomal frameshifting in mouse mammary tumor virus. *Nucleic Acids Res.* **25**, 1943–1949 (1997).
20. Szewczak, A.A., Moore, P.B., Chan, Y. & Wool, I.G. The conformation of the sarcin/ricin loop from 28S ribosomal RNA. *Proc. Natl. Acad. Sci. USA* **90**, 9581–9585 (1993).
21. Cate, J.H. *et al.* RNA tertiary structure mediation by adenosine platforms. *Science* **273**, 1696–1699 (1996).
22. Legault, P., Li, J., Mogridge, J., Kay, L.E. & Greenblatt, J. NMR structure of the bacteriophage lambda N peptide/box B RNA complex: Recognition of a GNRA fold by an arginine-rich motif. *Cell* **93**, 289–299 (1998).
23. Monzingo, A.F. & Robertus, J.D. X-ray analysis of substrate analogs in the ricin A-chain active site. *J. Mol. Biol.* **227**, 1136–1145 (1992).
24. Strobel, S.A. & Doudna, J.A. RNA seeing double: close-packing of helices in RNA tertiary structure. *Trends Biochem. Sci.* **22**, 262–266 (1997).
25. Chen, X. *et al.* A characteristic bent conformation of RNA pseudoknots promotes -1 frameshifting during translation of retroviral RNA. *J. Mol. Biol.* **260**, 479–483 (1996).
26. Gilson, M.K., Rashin, A., Fine, R. & Honig, B. On the calculation of electrostatic interactions in proteins. *J. Mol. Biol.* **184**, 503–516 (1985).
27. Peterson, R.D. & Feigon, J. Structural change in rev responsive element RNA of HIV-1 on binding rev peptide. *J. Mol. Biol.* **264**, 863–877 (1996).
28. Nicholls, A., Sharp, K.A. & Honig, B. Protein folding and association: insights from the interfacial and thermodynamic properties of hydrocarbons. *Proteins* **11**, 281–296 (1991).
29. Pullman, B. Electrostatics of polymorphic DNA. *J. Biomol. Struct. Dynam.* **1**, 773–794 (1983).
30. Young, M.A., Ravishanker, G. & Beveridge, D.L. A 5-nanosecond molecular dynamics trajectory for B-DNA: analysis of structure, motions, and solvation. *Biophys J.* **73**, 2313–2336 (1997).
31. Zakrzewska, K. & Pullman, B. Spermine–nucleic acid interactions: a theoretical study. *Biopolymers* **25**, 375–392 (1986).
32. Le, S.Y., Chen, J.H., Pattabiraman, N. & Maizel Jr., J.V. Ion-RNA interactions in the RNA pseudoknot of a ribosomal frameshifting site: molecular modeling studies. *J. Biomol. Struct. Dyn.* **16**, 1–11 (1998).
33. Suga, H., Cowan, J.A. & Szostak, J.W. Unusual metal ion catalysis in an acyl-transferase ribozyme. *Biochemistry* **37**, 10118–10125 (1998).
34. Correll, C.C., Freeborn, B., Moore, P.B. & Steitz, T.A. Metals, motifs, and recognition in the crystal structure of a 5S rRNA domain. *Cell* **91**, 705–712 (1997).
35. Kieft, J.S. & Tinoco, I. Solution structure of a metal-binding site in the major groove of RNA complexed with cobalt(III) hexamine. *Structure* **5**, 713–721 (1997).
36. Cate, J.H. & Doudna, J.A. Metal-binding sites in the major groove of a large ribozyme domain. *Structure* **4**, 1221–1229 (1996).
37. McDowell, J.A., He, L., Chen, X. & Turner, D.H. Investigation of the structural basis for thermodynamic stabilities of tandem GU wobble pairs: NMR structures of (rGGAGUUCC)2 and (rGGAUGUCC)2. *Biochemistry* **36**, 8030–8038 (1997).
38. Santalucia, J. & Turner, D.H. Structure of (rGGCGAGCC)2 in solution from NMR and restrained molecular dynamics. *Biochemistry* **32**, 12612–12623 (1993).
39. Wu, M. & Turner, D.H. Solution structure of (rGCGGACGC)2 by two-dimensional NMR and the iterative relaxation matrix approach. *Biochemistry* **35**, 9677–9689 (1996).
40. Holbrook, S.R., Sussman, J.L., Warrant, R.W., Church, G.M. & Kim, S. RNA-ligand interactions: (I) magnesium binding sites in yeast $tRNA^{phe}$. *Nucleic Acids Res.* **4**, 2811–2820 (1977).
41. Pyle, A.M. Role of metal ions in ribozymes. *Metal ions in biological systems* **32**, 479–520 (1996).
42. Hermann, T. & Westhof, E. Exploration of metal ion binding sites in RNA folds with Brownian dynamics simulation. *Structure* **6**, 1303–1314 (1998).
43. Gilson, M.K. & Honig, B. Calculation of the total electrostatic energy of a macromolecular system: solvation energies, binding energies, and conformational analysis. *Proteins* **4**, 7–18 (1988).
44. Lavery, R. & Pullman, B. The electrostaic field of DNA: the role of nucleic acid conformation. *Nucleic Acids Res.* **10**, 4383–4395 (1982).
45. Pley, H.W., Flaherty, K.M. & Mckay, D.B. Three-dimensional structure of a hammerhead ribozyme. *Nature* **372**, 68–74 (1994).